Motif of Two Coupled Phase Equations with Inhibitory Couplings as a Simple Model of the Half-Center Oscillator

Artyom Emelin, Alexander Korotkov, Tatiana Levanova(✉), and Grigory Osipov

Lobachevsky University, Nizhny Novgorod 603950, Russia
tatiana.levanova@itmm.unn.ru

Abstract. We propose a new simple model of the half-center oscillator (HCO) consists of two oscillatory neurons interacting via the inhibitory coupling. We found the regions of dynamics, typical for central pattern generators, in the parameter space of the model. Various bifurcation transitions between all these states are in the focus of the proposed study.

Keywords: Adler equation · Chemical synaptic coupling · Half-center oscillator · In-phase and anti-phase synchronization · Bifurcations

1 Introduction

Locomotor dynamics of animals is based on the rhythmic limb movements. It is well known that the basic rhythmic pattern of flexion-extension alternation can be generated in absence of any inputs by neural circuits known as central pattern generators (CPGs) [3,9,10]. It is widely accepted that such rhythmic activity involves reciprocal inhibitory couplings between neuronal ensembles. Nevertheless, the precise topology of the CPG circuits in many animals and in humans, as well as the mechanisms of rhythmogenesis and control of locomotor pattern, are not fully understood [2]. A large amount of experimental studies devoted to the organization of CPGs in experimental models allowed to formulate several general concepts of rhythm generation.

The most widely used hypothesis on the organization of locomotor CPG is based on the classical half-center model that was proposed by Brown [3] and further elaborated by others [11,16]. This concept suggests a quasi-symmetric organization of two half-center oscillators. Also, mutual inhibition for flexor-extensor alternation is critical for rhythmogenesis. A great amount of data collected from experimental studies also support the half-center hypothesis [5–18].

In this study we propose a new simple model of the half-center oscillator, which consists of two identical neurons coupled by chemical inhibitory synapses. The proposed mathematical model is described by two phase oscillators, each of them, without coupling, demonstrates regular oscillatory dynamics (spiking). We use the phase oscillator as a single unit because reproduction of temporal patterns, not the dynamics of an individual neuron, plays a crucial role [17] in the

D. Balandin et al. (Eds.): MMST 2022, CCIS 1750, pp. 82–94, 2022.
https://doi.org/10.1007/978-3-031-24145-1_7

paradigm of the half-centers. This approach pays tribute to the early modeling of animal locomotor CPG [4,6]. The elements are inhibitory coupled.

The paper is organized as follows. In Sect. 2 we introduce a model of the half-center oscillator which consists of two phase oscillators with inhibitory couplings. We investigate in Sect. 3 temporal patterns that can be observed in the system under study depending on different values of control parameters. Bifurcation transitions between these patters are also in the focus of the study. In Sect. 4 we discuss our findings, before we draw our conclusions.

2 The Model

Let us consider the model of a minimal neural ensemble consisting of two neuron-like elements coupled by inhibitory synaptic couplings as shown in the Fig. 1.

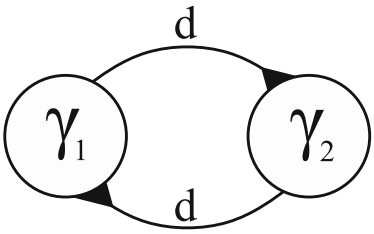

Fig. 1. Model of two oscillatory neurons with mutual inhibitory couplings.

To describe an individual element of an ensemble, we use the Adler equation [1]:

$$\dot{\phi} = \gamma - \sin\phi, \tag{1}$$

where the variable ϕ corresponds to the phase of an individual element, and γ is a parameter that determines the type of neuron behavior. For example, for $\gamma < 1$ in the phase space of the system, which is a unit circle, there are two equilibria: stable and unstable ones, which corresponds to the unexcited state of the neuron (Fig. 2(a)). When $\gamma = 1$, a saddle-node bifurcation occurs: both equilibria merge into one. In this case a neuron still remains unexcited, but now it can generate a single response on the external stimulus (Fig. 2(b)). Finally, for $\gamma > 1$, there are no equilibria in the phase space of the system, due to which the phase point begins to move counterclockwise along this circle. In this case if γ is slightly greater than 1, e.g. $\gamma = 1.01$, the neuron begins to generate spiking activity (Fig. 2(c)). Also, it should be noted, that (1) can be transformed to theta-neuron equation [8].

The connection between the elements will be specified using the $I(\phi)$ function, which, in accordance with biological principles, is specified in the following way:

$$I(\phi) = \frac{1}{1 + e^{k(\cos(\sigma) - \sin(\phi))}}. \tag{2}$$

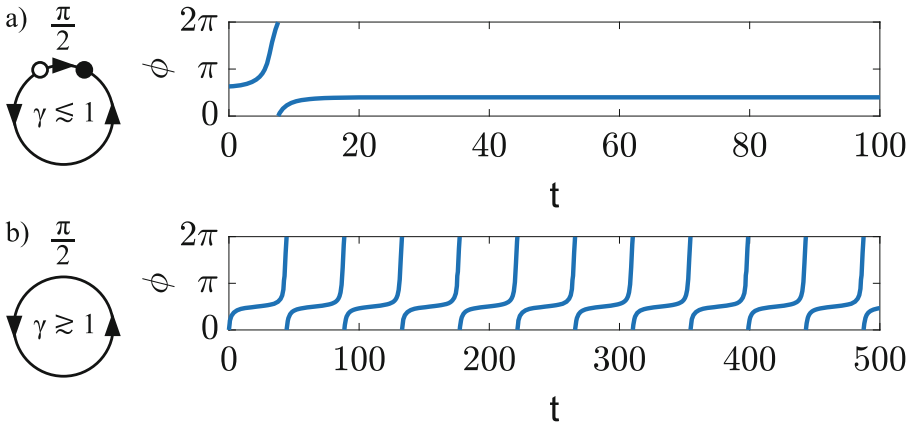

Fig. 2. Phase space and corresponding time series showing the saddle-node bifurcation in the Eq. (1). (a) For $\gamma < 1$, the system has stable and unstable equilibria, which corresponds to the absence of oscillations (unexcited state of the neuron) with the ability to generate activity with a small external stimulus. (b) If the value of the parameter $\gamma > 1$, there are no equilibria left in the system and the neuron generates spiking activity.

A coupling function of this kind was first introduced in [13] and then tested in [12,14,15]. Here we use its inhibitory analogue. This function simulates signal transmission from the presynaptic element to the postsynaptic element as follows. When the phase ϕ of the active presynaptic element reaches the value $\frac{\pi}{2} - \sigma$, this element stops inhibitory effect on the postsynaptic element. The duration of the cessation of the inhibitory effect is determined by the σ parameter and is 2σ. The dependence of the link function $I(\phi)$ on the phase of the presynaptic element ϕ is shown in the Fig. 3(a). It is important to note that this connection function takes into account the basic principles of the chemical interaction of neurons: (i) the presence or absence of activity of the postsynaptic element depends on the level of activity of the presynaptic element; (ii) all interactions between neuron cells are inertial due to the fact that signal transmission is not instantaneous. Using the σ parameter, which is responsible for the duration of the effect, we can simulate different types of couplings.

Thus, the system of two neuron-like phase elements with mutual synaptic inhibitory couplings is described by the following system of ordinary differential equations:

$$\begin{cases} \dot{\phi_1} = \gamma_1 - \sin\phi_1 - d \cdot I(\phi_2) \\ \dot{\phi_2} = \gamma_2 - \sin\phi_2 - d \cdot I(\phi_1) \end{cases} \tag{3}$$

where parameter d corresponds to the strength of inhibitory coupling $I(\phi)$. The phase space of (3) is torus (ϕ_1, ϕ_2). In this case, the regions where the inhibitory effect of the corresponding neurons stops are marked with blue and green areas in the Fig. 3(b).

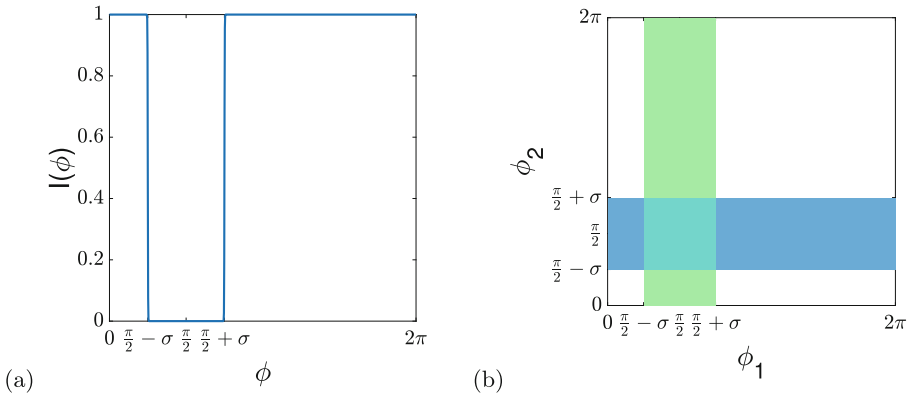

Fig. 3. (a) Type of inhibitory coupling function. (b) Regions on the phase torus in which the inhibitory effect of one element on another stops. In the green area, the first element ceases inhibit the second one. Similarly, in the blue area, the second element stops inhibitory effect on the first one. In the blue-green area, the mutual influence of elements on each other completely stops. (Color figure online)

3 The Results

In this section we study the case of identical elements. Each element is initially in a oscillatory activity, so we choose the values of natural frequencies slightly greater than one. To do this, we fix the parameters $\gamma_1 = \gamma_2 = 1.01$. We also fix the parameter $k = -500$, which is responsible for the switching speed in the coupling function (2). We will study the dynamics of the half-center oscillator by changing the parameter σ, which is responsible for the duration of the inhibitory effect, as well as the parameter d, which is responsible for the strength of the influence of elements on each other. It follows from the method of choosing the coupling function (2) that the parameter σ can take values from 0 to $\frac{\pi}{2}$. The values of the parameter of coupling strength d for biological reasons should not be chosen too large, since in this case the simulation will not be biologically relevant. Also, the parameter d obviously cannot take negative values. For the convenience of modeling, we assume that d can vary in the range from 0 to 1.5.

3.1 Maps of Temporal Patterns

To study and classify the dynamics in the system under consideration on the parameter plane $P = (\sigma; d)$, where $\sigma \in [0;\ \frac{\pi}{2}]$, $d \in [0;\ 1.5]$, two-parameter maps of neuron-like activity were obtained.

Let us note that initially, without couplings, both neuron-like elements demonstrated spiking activity. This situation corresponds to the parameter $d = 0$. Next, we consider how the dynamics of the system changes for different values of couplings parameters. To do this, we will study and describe each of the areas of neuron-like activity in the Fig. 4.

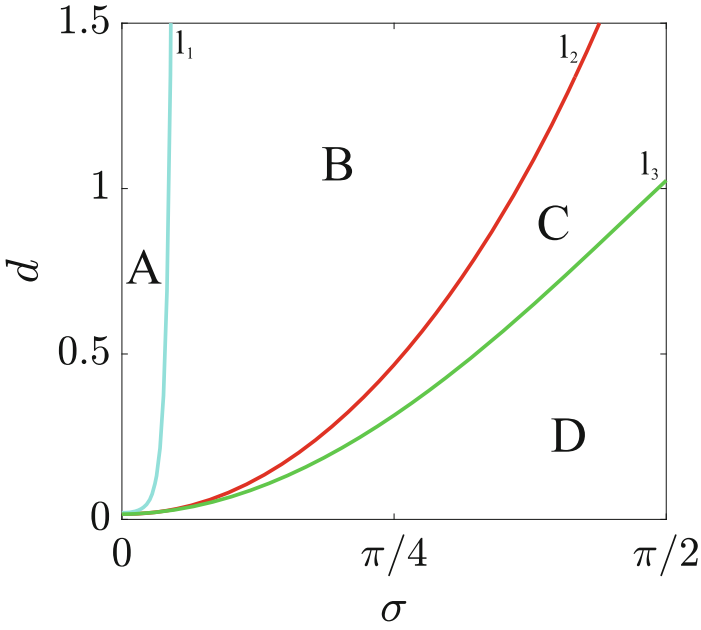

Fig. 4. Map of neuron-like temporal patterns in the system (3). Curves of different colors mark different bifurcation transitions. Curves l_1, l_3 correspond to a saddle-node bifurcation, and l_2 to a heteroclinic one. Regions A and B doesn't show any spiking activity and demonstrate only silence temporal pattern, sub-threshold oscillations or both. The next region C is characterized by the fact that the regime of anti-phase oscillations is added to the previously observed temporal patterns. In the case of D, only two temporal patterns remain in phase space: anti-phase spiking pattern and in-phase spiking pattern.

Next, some implementations of phase portraits and their corresponding time series will be demonstrated. Let us define some notation. Thus, on the phase portraits, dots of different colors mark the states of equilibria, namely:

- The red dot with a red outline is the saddle state of equilibrium.
- A pink dot with a purple outline is a state of equilibrium of the center type.
- The blue dot with a dark blue outline is a stable node.
- The blue dot with a red outline is an unstable node.
- A gray dot with a black outline is a complex equilibrium state.

Further, the pale red curves represent the vector field. In the phase portrait, the solid or dashed blue trajectories marks the trajectory calculated according to some initial conditions and correspond to blue (phase ϕ_1) and red (phase ϕ_2) solid or blue and red dashed ones on the time series respectively. The beginning of such a trajectory is marked with a dark blue dot. The time series of the corresponding trajectory is also shown to the right of the phase portrait. Finally, the areas where the inhibitory effect on the corresponding elements ceases are marked in green.

Let us list the types of neuron-like activity that can be observed in different regions from Fig. 4. The dynamics in region A is rather simple and corresponds to silence regime (absence of spikes). All other regions in the map Fig. 4 are regions of multistability, i.e. in this case several attractors coexist in the phase space of the system (3). In region B in addition to silence regime one can observe sub-threshold oscillations. Region C is characterized by three types of neuron-like temporal patterns: absence of oscillations, sub-threshold oscillations and anti-phase spiking. The region D features both anti-phase and in-phase spiking regimes.

Let us have a closer look at each of described regions in Fig. 4 and transitions between observed types of temporal activity patterns.

In the region A, the system (3) is characterized by the smallest area of interaction between elements in the ensemble. In this case, the system is able to demonstrate only the absence of activity (silence temporal pattern, see Fig. 5 (a, b)), since there are only four equilibria in its phase space, namely: a stable and unstable nodes, as well as two saddles.

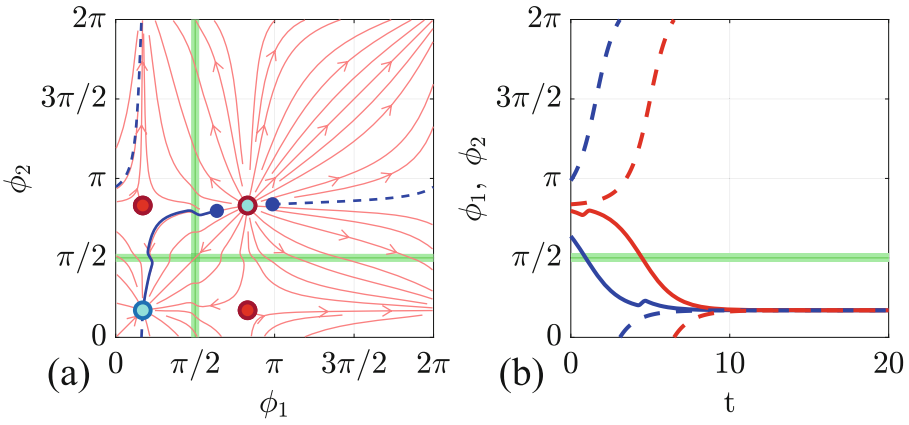

Fig. 5. (a) Phase portrait for the region A, demonstrating the silence temporal pattern. Here $\sigma = 0.08,\ d = 0.5$.(b) Time series for the first trajectory (blue and red solid lines represent phases ϕ_1 and ϕ_2 respectively) starting from $\phi_1^0 = 2,\ \phi_2^0 = 2.5$ and for the second trajectory (blue and red dashed lines represent phases ϕ_1 and ϕ_2 respectively) starting from $\phi_1^0 = 3.2,\ \phi_2^0 = 2.7$. (Color figure online)

The transition from region A to the region B occurs when crossing the curve l_1. When the parameter σ reaches the bifurcation value, a complex equilibrium state is formed with zero eigenvalues at the point with coordinates $(\phi_1, \phi_2) = (\frac{\pi}{2};\ \frac{\pi}{2})$. Which the value of σ increases further, complex one splits into two equilibria of the type center and two saddle ones (Fig. 6).

As a result, in addition to the silence regime (Fig. 7(a, b)), a sub-threshold oscillations also appear (Fig. 7(c, d)). Note, however, that the amplitude of these

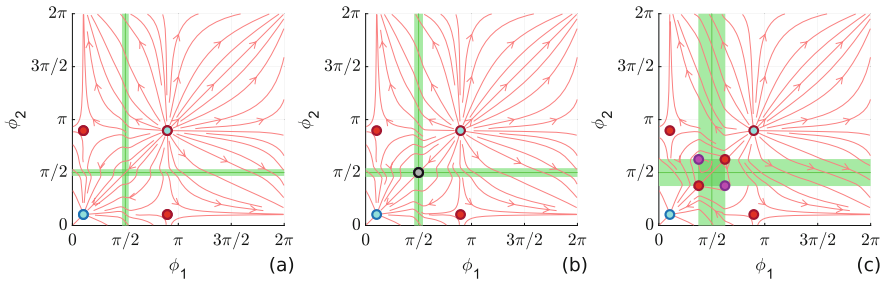

Fig. 6. Phase portraits showing the transition through the l_1 curve corresponding to the saddle-node bifurcation. The phase portraits are plotted for a fixed parameter $d = 0.6896$ and different values of the parameter σ: (a) $\sigma = 0.05$, (b) $\sigma = 0.13$, (c) $\sigma = 0.5$. (Color figure online)

sub-threshold oscillations is significantly less than the spike amplitude, i.e., it does not exceed the value of 2π. Thus, there is no spiking activity in the region B. From the point of view of constructing a dynamical model of HCO, the region B does not differ significantly from the previously considered region A.

Moving towards a further increase in the value of the σ, we cross the l_2 heteroclinic bifurcation curve and get into the C region. In this case, the separatrices of the saddles merge, forming two heteroclinic trajectories, which subsequently form a channel, leading to the occurrence of periodic trajectories inside it that correspond to anti-phase oscillations (Fig. 8). Such oscillations are called spikes and correspond to the rotator temporal pattern. The width of the resulting channel is determined by the value of the parameter σ.

Let us note that in the region C the multistability takes place: different temporal patterns coexist, including silence regime (Fig. 9(a, b)), anti-phase spiking (Fig. 9(c, d)) and sub-threshold oscillations (Fig. 9(e, f)).

Finally, by sufficiently increasing the parameter σ, we intersect the curve of the saddle-node bifurcation l_3 and get into the region D. During the bifurcation at the l_3 boundary, two centers, a stable and an unstable node with saddles, merge pairwise, resulting in the formation of four complex equilibrium states, which subsequently disappear (Fig. 10).

The region D is also a region of multisatbility, and the system strongly depending on the initial conditions. In that case only two temporal patterns remain in phase space: anti-phase spiking pattern (Fig. 11(a, b)) and in-phase spiking pattern (Fig. 11(c, d)).

3.2 Analytical Study of Bifurcation Transitions

Let us describe the bifurcation scenarios for the appearance and disappearance of various temporal patterns of neuron-like activity that are observed at the boundaries between regions in Fig. 4.

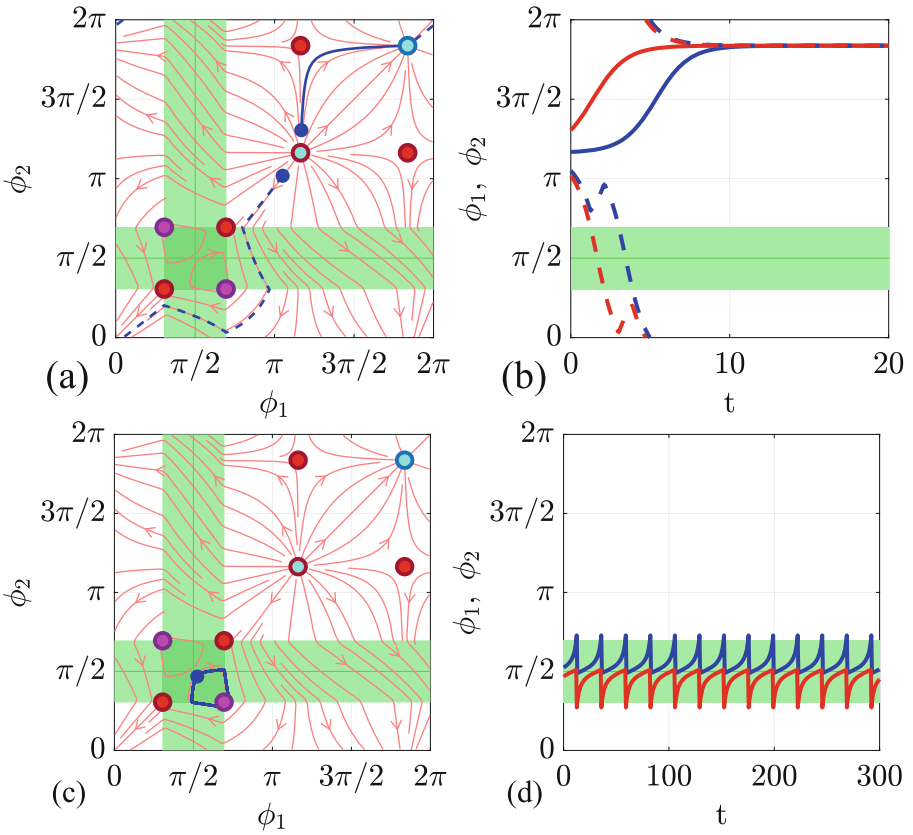

Fig. 7. Phase portraits and time series for the region B, demonstrating the silence regime (absence of oscillations) (a), (b) and sub-threshold oscillations (c), (d). Here $\sigma = 0.6171$, $d = 1.5$. In the phase portrait, the solid or dashed blue trajectories correspond to blue (phase ϕ_1) and red (phase ϕ_2) solid or blue and red dashed ones on the time series respectively. (Color figure online)

The equilibrium states of the system can be found from the following system of equations:

$$\begin{cases} \gamma_1 - \sin\phi_1 - d \cdot I(\phi_2) = 0 \\ \gamma_2 - \sin\phi_2 - d \cdot I(\phi_1) = 0 \end{cases} \tag{4}$$

Eigenvalues of equilibrium states can be found from the equation:

$$\lambda_{1,2} = \frac{-(\cos\phi_1 + \cos\phi_2) \pm \sqrt{(\cos\phi_1 - \cos\phi_2) + 4d^2 I'(\phi_1) I'(\phi_2)}}{2} \tag{5}$$

Equilibrium states of the first type $\phi_1 = \phi_2 = \phi$. Let us write down the conditions under which a saddle-node bifurcation occurs for such equilibrium states:

$$\begin{cases} \gamma - \sin(\phi) - I(\phi) = 0 \\ -\cos(\phi) \pm dI'(\phi) = 0 \end{cases} \tag{6}$$

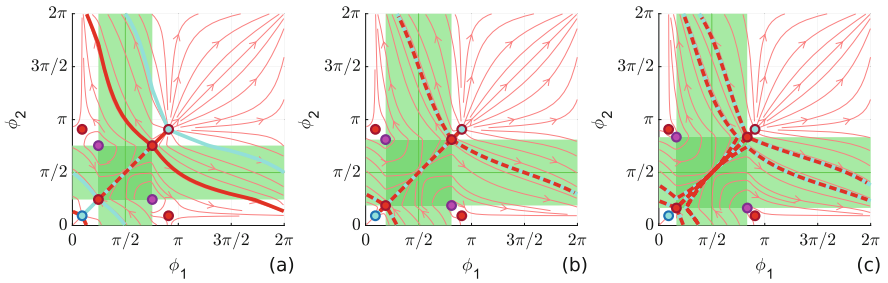

Fig. 8. Scenario of birth of the anti-phase limit cycle via the heteroclinic bifurcation. The separatrices of one saddle are marked with red color, and the separatrices of the other are marked with blue color. Heteroclinic trajectories are marked with red-blue marker. The phase portraits are plotted for a fixed parameter $d = 0.8$ and various parameters σ: (a) $\sigma = 0.9177$, (b) $\sigma = 1.025$, (c) $\sigma = 1.1507$. (Color figure online)

We transform the second equation and get

$$\cos(\phi)(-1 \pm dk\frac{e^{k(\cos(\sigma)-\sin(\phi))}}{1+e^{k(\cos(\sigma)-\sin(\phi))}}) = 0 \tag{7}$$

This relation shows that the equilibrium state $\phi = \frac{\pi}{2} + \pi k, k \in Z$ is complex and has both zero eigenvalues. Substituting this value ϕ into the first equation of the system (6), we obtain an equation of bifurcation curve on the parameter plane (σ, d), which correspond to the curve l_1 in the Fig. 4. Thus, the equations will have the following form

$$d = (\gamma \pm 1)(1 + e^{k(\cos\sigma \pm 1)}) \tag{8}$$

Now consider the expression in the parentheses. For the values of the parameters $d \geq 0$ and $k << 0$, it is satisfied only for the case

$$-1 - dk\frac{e^{k(\cos(\sigma)-\sin(\phi))}}{(1+e^{k(\cos(\sigma)-\sin(\phi))})^2} = 0 \tag{9}$$

Using the replacement $A = e^{k(\cos(\sigma)-\sin(\phi))}$, provided $e^{k(\cos(\sigma)+1)} \leq A \leq e^{k(\cos(\sigma)-1)}$, we get

$$e^{k(\cos(\sigma)-\sin(\phi))} = \frac{-(2+dk) \pm \sqrt{(2+dk)^2-4}}{2} \tag{10}$$

Expressing $\sin\phi$ from this equation and substituting it into the first equation of the system (6), we get

$$\begin{cases} \gamma - \cos\sigma + \frac{1}{k}\ln\frac{-(2+dk)\pm\sqrt{(2+dk)^2-4}}{2} - \frac{2d}{-dk\pm\sqrt{(2+dk)^2-4}} = 0 \\ e^{k(\cos(\sigma)+1)} \leq \frac{-(2+dk)\pm\sqrt{(2+dk)^2-4}}{2} \leq e^{k(\cos(\sigma)-1)} \end{cases} \tag{11}$$

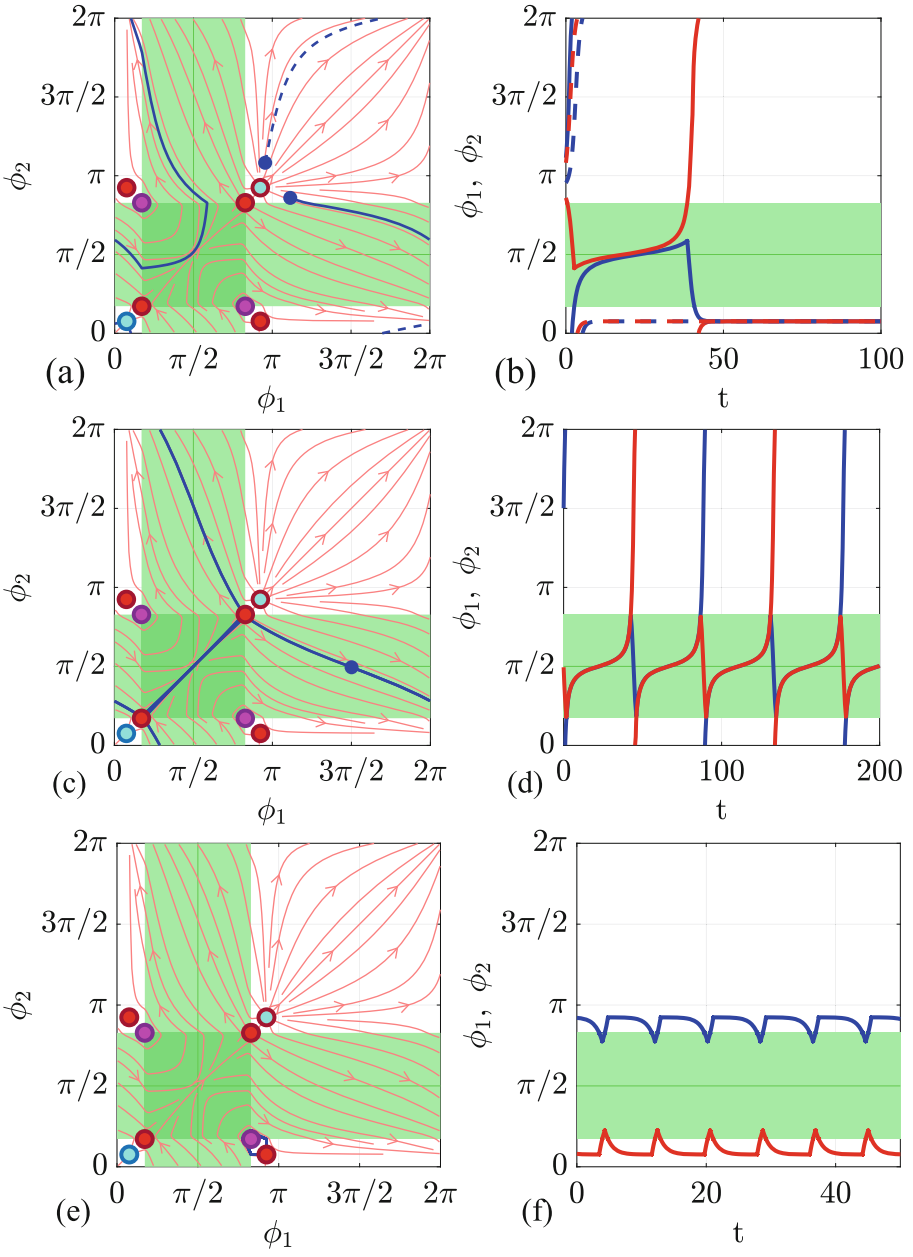

Fig. 9. Phase portraits and time series for the region C, demonstrating the silence regime (a), (b), anti-phase spiking (c), (d) and sub-threshold oscillations (e), (f). Here $\sigma = 1.0306,\ d = 0.7738$. In the phase portrait, the solid or dashed blue trajectories correspond to blue (phase ϕ_1) and red (phase ϕ_2) solid or blue and red dashed ones on the time series respectively. (Color figure online)

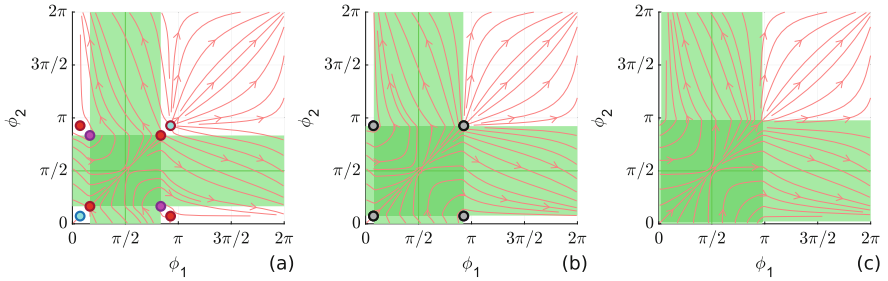

Fig. 10. Phase portraits showing the transition through the l_3 curve corresponding to the saddle-node bifurcation. The phase portraits were built for a fixed parameter $d = 0.8322$ and various parameters σ: (a) $\sigma = 1.1$, (b) $\sigma = 1.3777$, (c) $\sigma = 1.5$.

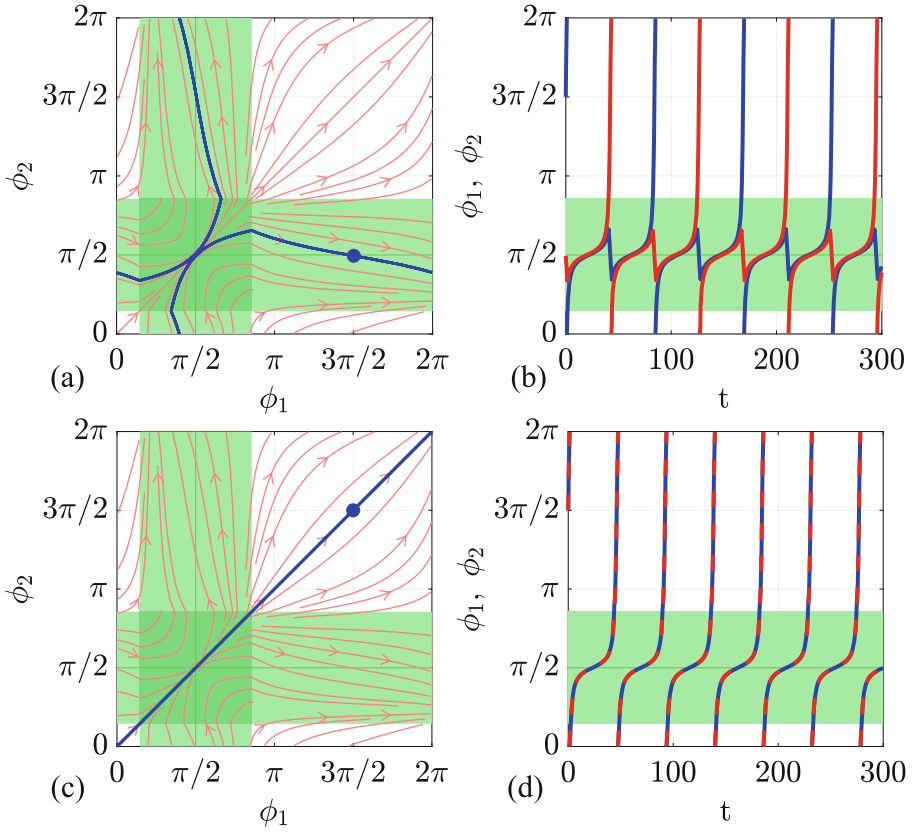

Fig. 11. Phase portraits and time series for region D, demonstrating anti-phase spiking (a), (b) and in-phase spiking (c), (d). Here $\sigma = 1.1175$, $d = 0.369$. In the phase portrait, the solid blue trajectory correspond to blue (phase ϕ_1) and red (phase ϕ_2) solid one on the time series. (Color figure online)

It can be verified numerically that the described system with given parameters is valid only for the case

$$\begin{cases} \gamma - \cos\sigma + \frac{1}{k}\ln\frac{-(2+dk)-\sqrt{(2+dk)^2-4}}{2} - \frac{2d}{-dk-\sqrt{(2+dk)^2-4}} = 0 \\ e^{k(\cos(\sigma)+1)} \le \frac{-(2+dk)-\sqrt{(2+dk)^2-4}}{2} \le e^{k(\cos(\sigma)-1)} \end{cases} \tag{12}$$

The resulting system of equations describes the curve l_3 in Fig. 4.

The l_2 curve was constructed numerically using the MatCont [7] mathematical package and corresponds to a heteroclinic bifurcation (Fig. 8).

In this case, before the bifurcation, stable separatrices come to the saddle from an unstable node, and unstable separatrices leaving the saddle tend to a stable node (Fig. 8(a)). As the parameter σ increases until it meets the curve l_2, a heteroclinic bifurcation occurs, during which unstable separatrices of one of the saddles become stable separatrices of the other saddle (Fig. 8(b)). Finally, after the σ parameter passes the l_2 curve and further increases, the heteroclinic trajectories between the saddles are preserved forming a channel (Fig. 8(c)).

4 Conclusion

In this study we have proposed a new phenomenological model of the HCO, consists of two oscillatory neurons coupled by chemical inhibitory synapses. On the one hand, it is simple and thus allows one to conduct analytical studies; on the other hand, despite its simplicity, it reflects the main properties of the biological HCO and reproduces all typical temporal patterns, including silent state, in-phase and anti-phase spiking. We have identified regions in the control parameters space that correspond to multistability, which support the hypothesis that the same pattern generator circuit can generate several types of neuron-like activity. We also have analyzed bifurcation transitions that lead to the occurrence of the specified temporal patterns.

This study may help one to gain new insights into the nature of the locomotor CPG and its functioning under different conditions. Namely, suggested model can be used as a building block of specific complex CPGs in studies of animal and robot locomotion.

Acknowledgements. This work was supported by the Ministry of Science and Education of Russian Federation (Project No. 0729-2020-0036).

References

1. Adler, R.: A study of locking phenomena in oscillators. Proc. IEEE **61**(10), 1380–1385 (1973)
2. Ausborn, J., Snyder, A.C., Shevtsova, N.A., Rybak, I.A., Rubin, J.E.: State-dependent rhythmogenesis and frequency control in a half-center locomotor CPG. J. Neurophysiol. **119**(1), 96–117 (2018)

3. Brown, T.G.: The intrinsic factors in the act of progression in the mammal. Proc. Roy. Soc. London Ser. B Containing Pap. Biol. Character **84**(572), 308–319 (1911)
4. Buono, P.L., Golubitsky, M.: Models of central pattern generators for quadruped locomotion I. Primary gaits. J. Math. Biol. **42**(4), 291–326 (2001)
5. Burke, R., Degtyarenko, A., Simon, E.: Patterns of locomotor drive to motoneurons and last-order interneurons: clues to the structure of the CPG. J. Neurophysiol. **86**(1), 447–462 (2001)
6. Cohen, A.H., Holmes, P.J., Rand, R.H.: The nature of the coupling between segmental oscillators of the lamprey spinal generator for locomotion: a mathematical model. J. Math. Biol. **13**(3), 345–369 (1982)
7. Dhooge, A., Govaerts, W., Kuznetsov, Y.A.: MATCONT: a MATLAB package for numerical bifurcation analysis of ODEs. ACM Trans. Math. Softw. (TOMS) **29**(2), 141–164 (2003)
8. Ermentrout, G.B., Kopell, N.: Parabolic bursting in an excitable system coupled with a slow oscillation. SIAM J. Appl. Math. **46**(2), 233–253 (1986)
9. Grillner, S.: Neurobiological bases of rhythmic motor acts in vertebrates. Science **228**(4696), 143–149 (1985)
10. Grillner, S.: Biological pattern generation: the cellular and computational logic of networks in motion. Neuron **52**(5), 751–766 (2006)
11. Jankowska, E., Jukes, M., Lund, S., Lundberg, A.: The effect of DOPA on the Spinal Cord 5. Reciprocal organization of pathways transmitting excitatory action to alpha motoneurones of flexors and extensors. Acta Physiol. Scand. **70**(3–4), 369–388 (1967)
12. Korotkov, A.G., Kazakov, A.O., Levanova, T.A.: Effects of memristor-based coupling in the ensemble of FitzHugh-Nagumo elements. Eur. Phys. J. Spec. Top. **228**(10), 2325–2337 (2019)
13. Korotkov, A.G., Kazakov, A.O., Levanova, T.A., Osipov, G.V.: Chaotic regimes in the ensemble of FitzhHugh-Nagumo elements with weak couplings. IFAC-PapersOnLine **51**(33), 241–245 (2018)
14. Korotkov, A.G., Kazakov, A.O., Levanova, T.A., Osipov, G.V.: The dynamics of ensemble of neuron-like elements with excitatory couplings. Commun. Nonlinear Sci. Numer. Simul. **71**, 38–49 (2019)
15. Korotkov, A.G., Levanova, T.A., Zaks, M.A., Maksimov, A.G., Osipov, G.V.: Dynamics in a phase model of half-center oscillator: two neurons with excitatory coupling. Commun. Nonlinear Sci. Numer. Simul. **104**, 106045 (2022)
16. Lundberg, A.: Half-centres revisited. In: Regulatory Functions of the CNS Principles of Motion and Organization, pp. 155–167. Elsevier (1981)
17. Sakurai, A., Newcomb, J.M., Lillvis, J.L., Katz, P.S.: Different roles for homologous interneurons in species exhibiting similar rhythmic behaviors. Curr. Biol. **21**(12), 1036–1043 (2011)
18. Yakovenko, S., McCrea, D., Stecina, K., Prochazka, A.: Control of locomotor cycle durations. J. Neurophysiol. **94**(2), 1057–1065 (2005)